Semi-active Control of Base-isolated Structures

Oliveira F., Gil de Morais P., Suleman A.

2015

Available online at www.sciencedirect.com

ScienceDirect

Procedia Engineering 114 (2015) 401 – 409

Procedia Engineering

www.elsevier.com/locate/procedia

1st International Conference on Structural Integrity

Semi-active control of base-isolated structures

Oliveira F.[a]*, Gil de Morais P.[a], Suleman A.[b,c]

[a]National Laboratory for Civil Engineering (LNEC), Av. do Brasil 101, 1700-066 Lisboa, Portugal
[b]University of Victoria, Department of Mechanical Engineering, PO Box 1700, Stn. CSC, Victoria, BC, V8W 2Y2, Canada
[c]Institute of Mechanical Engineering (IDMEC/IST), Av. Rovisco Pais 1, 1049-001 Lisboa, Portugal

Abstract

A numerical and experimental analysis of semi-active (SA) control strategies for controlling seismic-excited structures is presented. A physical model consisting of a two degree-of-freedom (2DOF) mechanical system with a magneto-rheological (MR) damper was developed to evaluate this concept at LNEC's shaking table. Linear elastic and viscous models were used to describe the mechanical behavior of the 2DOF mechanical system. A Modified Bouc-Wen model was used to describe the behavior of the MR damper. Four distinct control strategies were implemented for numerical and experimental evaluation. The associated controllers were tuned using the system model and the ground motions information. The strategies were the integral control law, two linear quadratic regulator strategies and a predictive controller, in conjunction with a clipped on-off algorithm. In both the numerical and experimental tests the results reveal that the response of the structure is effectively mitigated by all of the analyzed control methods. It is shown that SA systems can outperform the original structure as well as one using the best passive solution for most of the strategies. The integral control law exhibits the best performance when collocated control was considered. If more responses are available for control, the linear quadratic regulator technique exhibits even better performance.

Peer-review under responsibility of INEGI - Institute of Science and Innovation in Mechanical and Industrial Engineering

Keywords: semi-active control; integral controller; linear quadratic regulator; predictive control; seismic hazard mitigation; hybrid base-isolation.

1. Introduction

Civil engineering structures design has always been a challenge. Structures of main importance, such as hospitals, energy power stations, communication centers, civil protection and fire station buildings, which are vital to be kept operational during and immediately after the occurrence of an earthquake require a special attention in designing.

* Corresponding author. Tel.: +351-218-413-474; fax: +351-214-413-041.
E-mail address: fvoliveira@lnec.pt

Peer-review under responsibility of INEGI - Institute of Science and Innovation in Mechanical and Industrial Engineering
doi:10.1016/j.proeng.2015.08.085

Thus, innovative systems for structural protection of structure when subjected to earthquakes have been developed: passive, semi-active (SA), active and hybrid systems [1,2].

A particular type of passive system that has been commonly implemented recently is the base isolation concept. The idea consists in decoupling the main structure (superstructure) from the foundation in order to reduce the potential for structural damage and increase equipment safety by reducing the transmission of seismic forces and energy to the main structure [3]. Base-isolated structures with semi-active systems (hybrid systems) have been receiving much attention in recent years for improving the performance of structures against earthquake loads [4,5]. Magneto-rheological (MR) and fluid viscous dampers (FVD) are some of the typical semi-active devices used in these situations [6,7]. The idea consists in changing the damping characteristics in real time between an upper and a lower limit by offering similar reliability to passive control devices and maintaining the adaptability of active control systems with low power requirements [2,7]. Although very attractive in terms of energy consumption and generated forces, when as associated with the structure leads to a nonlinear system (structure plus device) with bounded inputs. The analysis and design can be performed using a set of available procedures: i) Lyapunov based methods [8,9]; ii) maximum energy dissipation algorithm and the modulated homogeneous friction algorithm [8,10]; iii) sliding mode control [11]; iv) quantitative feedback theory and backstepping control technique [12]; v) intelligent paradigms, like neural networks or fuzzy-logic [13]; vi) and force-tracking, consisting of a controller to derive a desired force and an algorithm to adjust the control variable, like optimal control [8,13], proportional plus integral control [14] or the force derivative feedback control [15], are typical controllers used for this purpose.

For this work a numerical and experimental analysis of semi-active (SA) control strategies for controlling seismic-excited structures was performed. Several control strategies were examined and compared with the best passive case. A physical model consisting of a two degree-of-freedom (2DOF) mechanical model with MR damper was developed to evaluate this concept at LNEC's shaking table. Numerical and experimental results obtained for the original structure and for passive cases were used for comparison with the SA cases, in terms of performance resulting from several input ground motions The experience accumulated in designing semi-active systems can be used to implement the technology in real civil engineering structures.

2. Structural System and control device

The structural model developed (Fig.1) is a 2DOF mechanical system representative of typical base isolated buildings excited by one dimensional earthquake loads, consisting of two masses (m_i & m_s) and two springs (k_i & k_s). The model is intended to reproduce the characteristics of a typical base isolated building, a typical 10-storey dual frame-wall structure with a fundamental frequency f_{s1}=1,6 Hz and a structural damping ratio of ξ_1=5 % (first mode, fixed base characteristics) supported on a base isolation system with a mass m_b=1,4·m_f (with m_f as the mass of each floor) and laminated rubber bearings with a target frequency f_b=0,4 Hz and an equivalent damping ratio of ξ_b=10 %, which are representative of typical base isolated structures. A MR damper was attached between the ground and mass m_i to increase the system damping. This device was operated by the data acquisition and control system using the information provided by the sensors, i.e. 1 force transducer (MR damper force measurement), 3 accelerometers (input ($\ddot{x}_g$), mass m_i ($\ddot{x}_i$) and mass m_s ($\ddot{x}_s$) accelerations) and 3 displacement transducers (input (x_g) displacement, relative displacement between mass m_i and ground (x_{ig}) and relative displacement between mass m_s and mass m_i (x_{si})). The reference signal for the shaking table was also defined on the data acquisition and control system. This equipment also allows the implementation of the control strategies and the measurement of the intended quantities. A schematic view of the system, as well as the developed mechanical model and the corresponding discretized model are depicted in Fig.1.

2.1. 2DOF model

The 2DOF model was developed in order to mach the first two modal characteristics (frequency and damping ratio) as well as the anti-resonance (fixed base frequency) were similar with the ones of the base isolated building. It consists of two springs having a total stiffness k_i that link the ground to mass m_i, and second pair of springs with a total stiffness k_s that link the mass m_i to mass m_s. The masses are supported by roller bearings over the shaking table

platform. The system damping will result from the damping associated with this mechanism that shall be due mainly to the rolling friction.

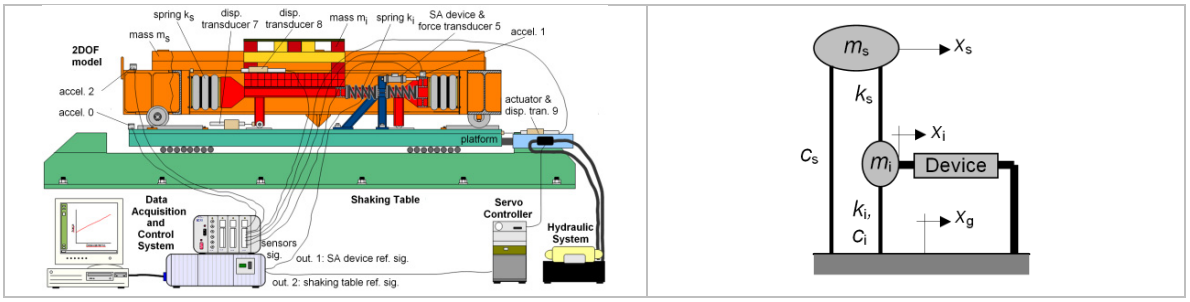

Fig. 1. Mechanical model: (a) schematic view; (b) and 2DOF equivalent model.

The springs were tested in a universal testing machine where the force and displacement were measured using a traceable measurement chain. Springs k_i have around 180 mm of diameter, 370 mm of free length, a coil diameter of 13.5 mm, and were tested in compression in the range of 190 mm and 3.5 kN. Both springs k_s have a free length and diameter around 300 mm, a coil diameter around 38 mm, and were tested in compression up to 90 mm and 19 kN. The linear model $f=k\cdot x$ fit well to the data obtained. The values were: k_i=33.8 N/mm; k_s=406.9 N/mm. Masses m_i and m_s were adjusted to fit the intended natural frequencies, resulting in: m_i=1790 kg; and m_s=3950 kg.

The equations of motion that describe the mechanical behavior of the 2DOF structural system in the spatial form as well as the model described in the state-space form are:

$$\begin{aligned} &\boldsymbol{M}_s\cdot\ddot{\boldsymbol{x}}_{rg}+\boldsymbol{C}_s\cdot\dot{\boldsymbol{x}}_{rg}+\boldsymbol{K}_s\cdot\boldsymbol{x}_{rg}=-\boldsymbol{M}_s\cdot\boldsymbol{1}\cdot\ddot{x}_g+\boldsymbol{G}\cdot f_{ad},\ \text{w/}\boldsymbol{M}_s=\begin{bmatrix} m_i & 0\\ 0 & m_s\end{bmatrix},\boldsymbol{K}_s=\begin{bmatrix} k_i+k_s & -k_i\\ -k_s & k_s\end{bmatrix},\boldsymbol{C}_s=\begin{bmatrix} c_i & 0\\ 0 & c_s\end{bmatrix},\boldsymbol{G}=\begin{bmatrix}-1\\ 0\end{bmatrix}\\ &\begin{aligned}\dot{\boldsymbol{z}}&=\boldsymbol{A}\cdot\boldsymbol{z}+\boldsymbol{B}\cdot f+\boldsymbol{E}\cdot\ddot{x}_g\\ \boldsymbol{y}&=\boldsymbol{C}\cdot\boldsymbol{z}+\boldsymbol{D}\cdot f_{ad}\end{aligned},\ \boldsymbol{E}=\begin{bmatrix}\boldsymbol{0}\\ \boldsymbol{-1}\end{bmatrix},\ \text{w/}\boldsymbol{A}=\begin{bmatrix}\boldsymbol{0} & \boldsymbol{I}\\ -\boldsymbol{M}_s^{-1}\cdot\boldsymbol{K}_s & -\boldsymbol{M}_s^{-1}\cdot\boldsymbol{C}_s\end{bmatrix},\ \boldsymbol{B}=\begin{bmatrix}\boldsymbol{0}\\ \boldsymbol{M}_s^{-1}\cdot\boldsymbol{G}\end{bmatrix}\end{aligned} \tag{1}$$

where: $\boldsymbol{M}_s$, $\boldsymbol{C}_s$ and $\boldsymbol{K}_s$ are the mass, damping and stiffness matrices respectively; $\boldsymbol{1}$ is a unitary column vector; f_{ad} is the force provided by an additional device installed at the base; $\ddot{x}_g$ is the input absolute acceleration at the base (ground); and $\boldsymbol{x}_{rg}=\{x_{ig}\ x_{sg}\}^T$ is the vector of relative displacements of the DOF to the ground: $x_{ig}=x_i-x_g$; $x_{sg}=x_s-x_g$; $\boldsymbol{z}=\{\boldsymbol{x}_{rg}\ \dot{\boldsymbol{x}}_{rg}\}^T$ is the state vector; $\boldsymbol{y}$ is the output vector defined according to the quantity required for output through the matrices $\boldsymbol{C}$ and $\boldsymbol{D}$; $\boldsymbol{0}$ is a null matrix or a null vector and $\boldsymbol{I}$ is the identity matrix. A damping matrix proportional to the mass is assumed since the developed physical model dissipative forces are mainly due to the rolling friction located at those DOFs.

The physical model was installed on the shaking table as depicted in figure Fig. 1, without the SA device, and was subjected to a campaign of tests in order to identify its modal properties. A white-noise signal (duration of 360 s passed through a higher-pass filter at 0,2 Hz and integrated once) was used as the reference displacement for the shaking table (peak values of 22 mm/7.1 m/s^2). Scale factors from 0.6 to 1 were applied to the reference signal. The frequency response functions (FRFs) were evaluated (H1 estimator) using the measured time data and the results can be found in Fig. 2(a). A small dependence of the input magnitude on the system behavior, namely on the natural frequencies and damping is observed. To identify the system modal properties, the experimental model consisting on the frequency response functions in terms of accelerations and relative displacements to the ground, were used to obtain the parameters of the continuous time model in equation (1). The prediction-error minimization method available at Matlab was used for that purpose. A Rayleigh damping model ($\boldsymbol{C}_s=\alpha\cdot\boldsymbol{M}_s$) was used to describe the dissipative mechanism. In the identification process the model parameters m_i and m_s were assumed to be invariant and the other parameters, k_i, k_s, c_i and c_s were the selected unknown. From the identified modal properties: f_1=0.4 Hz; ξ_1=5.2 %; f_2=3.03 Hz; and ξ_2=0.7 %; the resulting identified model parameters were: m_i=1790 kg; and m_s=3950 kg;

k_i=3.8x10^4 N/mm; and k_s=4.3x10^5 N/mm; and α=0.3 /s. A comparison between the experimental FRFs and the regenerated ones using the mathematical model with the identified parameters can be found in Fig. 2(b), for the maximum input signal magnitude. A good agreement is found between the experimental and the spatial model data.

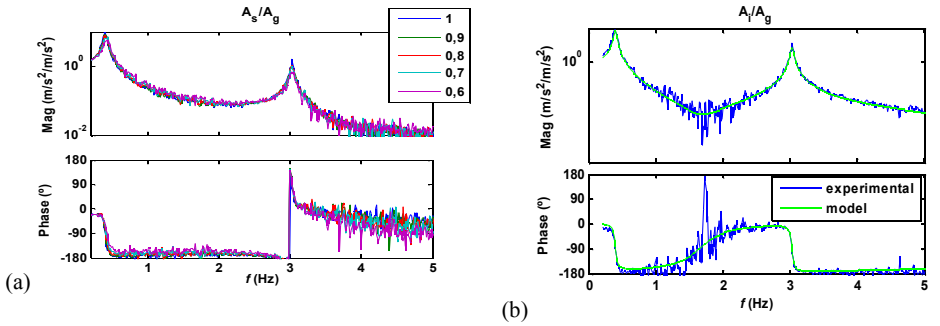

Fig. 2. Frequency Response Functions (FRFs): (a) experimental FRFs; (b) comparison between the experimental and the regenerated FRFs.

2.2. SA device

A MR damper model RD-8041-1 with a current controller RD-3002-03 manufactured by LORD Corporation (http://www.lord.com) was used as the SA device in this work. The damper has a stroke of 74 mm and can reach up to 1.5 kN at 0.2 m/s for a current in the coils of around 2 A. A constant voltage power supply capable of producing at least 2 A of current was used.

To describe the mechanical behavior of the damper the Modified Bouc-Wen model [16] was used:

$$\begin{cases} f_{ad} = \begin{cases} k_0 \cdot (x_r - y) + k_1 \cdot x_r + c_0 \cdot \dot{x}_r + k_w \cdot w + f_0 \\ c_1 \cdot \dot{y} + k_1 \cdot x_r + f_0 \end{cases} \\ \dot{w} = \rho \left[(\dot{x}_r - \dot{y}) - \sigma \cdot |\dot{x}_r - \dot{y}| \cdot w \cdot |w|^{n-1} + (\sigma - 1) \cdot (\dot{x}_r - \dot{y}) \cdot |w|^n \right] \\ \dot{V}_{eq} = \dfrac{1}{\tau}(V - V_{eq}) \end{cases} \quad (2)$$

where: k_0 is an elasticity due to the internal accumulator used to compensate the volume variations in single ended dampers; f_0 is an offset force due to the accumulator, for the same reason; c_0 is the post-yield damping coefficient; k_w is the yield force; ρ, σ and n are parameters used to model the hysteresis loop; x_r is the relative displacement between damper ends; $w \in [-1,1]$ is an internal variable (normalized) used to describe the force-velocity hysteresis; parameters k_1 and c_1 as well as the variable y are used to model the force roll-off at lower velocities. The different magnetic field strengths will be achieved by the dependence of some parameters with the applied input voltage V and relative velocity v: $c_0(V,v)$; $c_1(V,v)$; $k_w(V,v)$; $\rho(V,v)$; $\sigma(V,v)$; in the stationary regime $V=V_{eq}$, to account for the transient response of the device, a first order dynamic model is introduced through a time constant τ.

In order to characterize the mechanical behavior of the assembly (damper plus current controller) several tests were performed: i) static tests at several displacement points to identify the static components of the device; ii) dynamic tests, under a stationary regime in the whole displacement range, and under a transient regime, to identify the stationary and transient components of the device. The tests were performed on a universal testing machine as depicted in Fig. 3(a). The ***static test*** consisted in the application of three displacement cycles between -34 mm and 34 mm in steps of 8.5 mm and from the force-displacement data the following values were identified: stiffness k_1=0.987 N/mm; and the offset force f_0=-139.831 N. The ***dynamic tests in the stationary regime*** consisted in subjecting the device to sinusoidal displacement waves (10 cycles of 6.25, 12.5 and 25 mm amplitude with frequencies from 0.25 Hz to 2 Hz) and from the force-displacement and force-velocity data identify the Modified

Bouc-Wen model parameters: n=2; k_0=10-4 kN/m; $c_0(V,v)$=[0.001-0.015] kN·s/mm; $c_1(V,v)$=[0.01-0.5] kN·s/mm; $k_w(V,v)$=[0.1-1.2] kN; $\rho(V,v)$=[2-20] /mm; $\sigma(V,v)$=[0.1-12]; for these last parameters a set of tables relating the model parameters with the input voltage and peak velocity were implemented, and intermediate values were calculated using linear interpolation. The ***dynamic tests under the transient regime*** used a triangle displacement signal and imposed step voltage to the damper between inversions (12,5 mm of amplitude, frequencies from 0.25 Hz to 0.75 Hz, and input steps from 0 V to 5 V and 5 V to 0 V) to identify the response time of the damper. The average time constant taking into account all the tests was found to be τ=21 ms. After model parameterization the model a comparison between the experimental data and the model data was performed, as depicted in Fig. 3(b), showing a good agreement between experimental and numerical data.

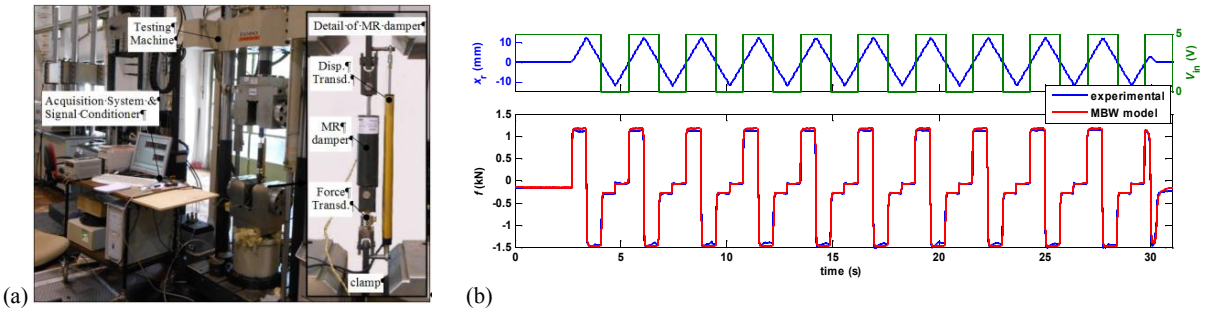

Fig. 3. (a) Set-up of the experimental test; (b) Comparison between the measured MR damper force and the force evaluated by the model.

3. Semi-Active controllers

The semi-active controllers considered in this study were: ICOO – integral controller with an on-off algorithm; LQRCOO and LQR2COO – linear quadratic regulators with an on-off algorithm; MPCCOO – Model predictive controller with an on-off algorithm. These controllers are of the force feedback type, which use a linear controller to calculate a desired force f_d, using the feedback information (measured responses), which is then used to compute (algorithm) the input voltage V of the device using the feedback information of the device (measured force). The following sub-sections describe the SA controllers.

3.1. ICOO

The output of the controller or the desired force f_d is given as:

$$f_d = -g\int_0^{\tau} \ddot{x}_i(\tau)\,d\tau = -g\cdot\dot{x}_i \tag{3}$$

where: g is the controller gain; $\ddot{x}_i$ and $\dot{x}_i$ are the absolute acceleration and velocity at the base floor respectively.

The control variable, i.e. the input voltage for the MR damper is calculated using a clipped on-off algorithm [8] using the Heaviside step function H[·]:

$$V = V_{max}\cdot H\left[\left(f_d - f_{ad}\right)\cdot f_{ad}\right],\ 0 \le V \le 5\,V \tag{4}$$

3.2. LQRCOO & LQR2COO

This controller computes a control signal that is proportional to states of the system. Assuming that the system is subjected to white noise excitation with zero mean E[w]=0 and known variance E[$w\cdot w^T$]=w_0, the performance index

that weights the output $\boldsymbol{y}$ and the input desired force f_d, the solution of the problem (i.e. the control force) and solution of the algebraic Riccati equation, are given by:

$$\begin{aligned} &J = \lim_{\tau\to\infty} \frac{1}{\tau} \mathrm{E}\left[\int_0^{\tau} \boldsymbol{y}^{\mathrm{T}} \cdot \boldsymbol{Q}_{\mathrm{y}} \cdot \boldsymbol{y} + r \cdot f_{\mathrm{d}}^2 \,\mathrm{d}t\right] \\ &f_{\mathrm{d}} = -\boldsymbol{K}_{\mathrm{C}} \cdot \boldsymbol{z}, \mathrm{w/} \boldsymbol{K}_{\mathrm{C}} = \boldsymbol{R}^{-1} \cdot \left[\boldsymbol{B}^{\mathrm{T}} \cdot \boldsymbol{P} + \boldsymbol{N}^{\mathrm{T}}\right] \\ &\boldsymbol{P} \cdot \boldsymbol{A} + \boldsymbol{A}^{T} \cdot \boldsymbol{P} - \left(\boldsymbol{P} \cdot \boldsymbol{B} + \boldsymbol{N}\right) \cdot \boldsymbol{R}^{-1} \cdot \left(\boldsymbol{B}^{\mathrm{T}} \cdot \boldsymbol{P} + \boldsymbol{N}^{\mathrm{T}}\right) + \boldsymbol{Q} = \boldsymbol{0}, \mathrm{w/} \boldsymbol{Q} = \boldsymbol{C}^{\mathrm{T}} \cdot \boldsymbol{Q}_{\mathrm{y}} \cdot \boldsymbol{C}, \boldsymbol{R} = r + \boldsymbol{D}^{\mathrm{T}} \cdot \boldsymbol{Q}_{\mathrm{y}} \cdot \boldsymbol{D}, \boldsymbol{N} = \boldsymbol{C}^{\mathrm{T}} \cdot \boldsymbol{Q}_{\mathrm{y}} \cdot \boldsymbol{D} \end{aligned} \tag{5}$$

where: $\boldsymbol{K}_c$ is the controller gain; $\boldsymbol{P}$ is the solution of the algebraic Riccati equation.

As in the previous strategy, the control variable is evaluated by equation (4). With LQRCOO strategy, a reduced version of the model in equation (1) accounting only the first mode of vibration is considered in the controller synthesis. The weighting variables are the mass m_i acceleration ($\ddot{x}_i$) and the input desired force (f_d). On the other hand, in LQR2COO the whole model in equation (1) is considered in the controller synthesis and the weighting variables are both accelerations ($\ddot{x}_i$ and $\ddot{x}_s$ w/equal gains) and the input desired force (f_d).

3.3. MPCCOO

A predictive controller was also considered here to evaluate the desired force of the device. The idea was to predict future outputs from actual measurements and past inputs using the system model (predictor), then compare the outputs with the reference and determine input trajectories (optimizer). The formulation for this controller was already presented in [17], whose solution is given by:

$$\Delta \boldsymbol{F}_{\mathrm{d}}(k) = \frac{1}{2} \boldsymbol{H}_{\mathrm{term}}^{-1} \cdot \boldsymbol{G}_{\mathrm{term}}, \mathrm{w/} \boldsymbol{H}_{\mathrm{term}} = \boldsymbol{\Theta}^{\mathrm{T}} \cdot \boldsymbol{Q}_{\mathrm{mpc}} \cdot \boldsymbol{\Theta} + \boldsymbol{R}_{\mathrm{mpc}}, \boldsymbol{G}_{\mathrm{term}} = 2 \cdot \boldsymbol{\Theta}^{\mathrm{T}} \cdot \boldsymbol{Q}_{\mathrm{mpc}} \cdot \boldsymbol{E}(k) \tag{6}$$

where: $\Delta \boldsymbol{F}_{\mathrm{d}}(k)$ is the vector of future force input moves at instant k; $\boldsymbol{\Theta}$ is the matrix function of the model parameters; $\boldsymbol{E}(k)$ is the tracking error at instant k; $\boldsymbol{Q}_{\mathrm{mpc}}$ and $\boldsymbol{R}_{\mathrm{mpc}}$ are weighting matrices. $\Delta f_{\mathrm{d}}(k)$ is the first term of $\Delta \boldsymbol{F}_{\mathrm{d}}(k)$ that will be used to evaluate the desired force $f_{\mathrm{d}}(k)=f_{\mathrm{d}}(k\text{-}1)+\Delta f_{\mathrm{d}}(k)$.

Again, as in the previous strategies the control variable is evaluated by equation (4), a reduced version of the model in equation (1) accounting only the first mode of vibration is considered and the weighting variables are the $\ddot{x}_i$ and Δf_{d}.

4. Results

Numerical simulations and experimental tests were performed in order to evaluate the performance of the system with each strategy. Several input ground motions were considered: Type 1 & 2 accelerograms for the Portuguese territory [17] and recorded ground motions [18]. Before laboratory experiments were carried out, numerical simulations were performed using the identified model and the specific semi-active control strategy to identify the best controller parameters. The minimum of mean peak mass m_s acceleration $\ddot{x}_s$ was the criteria used to identify the controller parameters. The following values were obtained: integral controller, g=13777 N/m; LQR, q=2x10^7 kg·s, r=1 s/kg; LQR2, q=1.17x10^7 kg·s, r=1 s/kg; MPC, q=1448 kg$^{0.5}$·s, r=1 s/kg$^{0.5}$. In table 1 are presented the results of numerical simulations and experimental trials resulting from a type 1 accelerogram, a type 2 accelerogram and the Kobe earthquake, at 15%, 32% and 13% of magnitude respectively. The results are presented in terms of ratios of peak responses of each variable for each solution in relation to the peak responses obtained with the original structural system (no devices): Rx_{ig}, and Rx_{si} for the relative displacement; Ra_i and Ra_s for the accelerations; Ra_o, average of the four ratios; for the original structure these parameters take the unitary value and the absolute peak values are also presented (in brackets). The ratio of peak force relative to the structure weight is also shown Pf/W. In the table are also presented the results for the damper in passive mode with 0 V, 1 V and 5 V, corresponding to the minimum passive case, the one for the minimum peak acceleration $\ddot{x}_s$, and the maximum passive case.

Looking into the data it can be observed that in general the passive solution with maximum input voltage Pass5 lead to the highest reductions at $\ddot{x}_{ig}$ but at the expense of increasing the other responses. The semi-active strategies perform better than the passive Pass1 case, and also better than the original structure.

Table 1. Results of Numerical and Experimental trials under the Portuguese Type 1 & Type 2 accelerogram and Kobe earthquake.

Case/Study	*Numerical*						*Experimental*					
	Rx_{ig}	Rx_{sg}	Ra_i	Ra_s	Ra_o	Pf/W	Rx_{ig}	Rx_{sg}	Ra_i	Ra_s	Ra_o	Pf/W
	Seismic Action Type 1											
Original	1 (47.33mm)	1 (3.19mm)	1 (0.352m/s^2)	1 (0.350m/s^2)	-	-	1 (63.44mm)	1 (4.02mm)	1 (0.511m/s^2)	1 (0.439m/s^2)	-	-
Pass0	0.67	0.73	**0.74**	0.75	**0.72**	0.000	0.42	0.62	**0.71**	0.71	**0.62**	0.004
Pass1	0.40	0.76	1.07	0.77	0.75	0.003	**0.31**	**0.66**	0.90	0.70	0.64	0.009
Pass5	**0.21**	1.60	2.48	1.62	1.48	0.006	**0.12**	1.28	1.30	1.43	1.03	0.031
ICOO	**0.37**	**0.47**	**0.86**	**0.48**	**0.55**	0.009	**0.30**	**0.44**	**0.64**	**0.49**	**0.47**	0.012
LQRCOO	0.42	**0.50**	**0.81**	**0.53**	**0.56**	0.012	**0.28**	**0.41**	**0.53**	**0.48**	**0.42**	0.009
MPCCOO	**0.40**	**0.63**	**1.05**	**0.65**	**0.68**	0.011	**0.30**	**0.53**	0.92	**0.66**	**0.60**	0.009
LQR2COO	0.41	**0.44**	**0.54**	**0.48**	**0.47**	0.011	**0.26**	**0.34**	**0.59**	**0.47**	**0.41**	0.011
	Seismic Action Type 2											
Original	1 (44.01mm)	1 (2.78mm)	1 (0.328m/s^2)	1 (0.307m/s^2)	-	-	1 (47.17mm)	1 (3.66mm)	1 (0.534m/s^2)	1 (0.391m/s^2)	-	-
Pass0	0.72	**0.78**	**0.98**	**0.75**	**0.81**	0.003	0.65	**0.55**	**0.68**	**0.62**	**0.63**	0.003
Pass1	0.41	0.79	1.47	0.85	0.88	0.006	0.33	0.59	1.02	0.70	0.66	0.005
Pass5	**0.15**	1.82	2.84	1.81	1.66	0.027	**0.13**	1.44	1.81	1.62	1.25	0.031
ICOO	**0.38**	**0.71**	**1.45**	**0.70**	**0.81**	0.012	**0.33**	**0.52**	**0.87**	**0.56**	**0.57**	0.014
LQRCOO	0.46	**0.77**	**1.26**	**0.83**	**0.83**	0.011	0.37	0.61	**0.81**	0.79	**0.65**	0.010
MPCCOO	**0.39**	**0.74**	**1.47**	**0.72**	**0.83**	0.010	0.38	**0.49**	**0.61**	**0.58**	**0.51**	0.005
LQR2COO	0.46	**0.65**	**1.33**	**0.64**	**0.77**	0.012	**0.31**	**0.40**	**0.73**	**0.56**	**0.50**	0.010
	Kobe Earthquake											
Original	1 (40.54mm)	1 (2.74mm)	1 (0.313m/s^2)	1 (0.288m/s^2)	-	-	1 (38.06mm)	1 (3.17mm)	1 (0.397m/s^2)	1 (0.331m/s^2)	-	-
Pass0	0.85	**0.83**	**0.89**	**0.89**	**0.86**	0.003	0.83	**0.82**	**0.89**	**0.89**	**0.86**	0.003
Pass1	0.61	0.89	1.67	0.99	1.04	0.007	0.74	0.82	1.64	0.90	1.02	0.006
Pass5	**0.47**	2.41	3.79	2.61	2.32	0.030	**0.53**	2.22	2.78	2.49	2.00	0.034
ICOO	**0.57**	**0.58**	**0.80**	**0.64**	**0.65**	0.013	**0.55**	**0.58**	**0.82**	**0.66**	**0.65**	0.015
LQRCOO	**0.60**	**0.80**	**1.28**	**0.87**	**0.89**	0.017	**0.54**	**0.76**	**0.92**	**0.89**	**0.78**	0.016
MPCCOO	0.68	**0.79**	**1.07**	**0.85**	**0.85**	0.011	**0.67**	**0.62**	**0.99**	**0.80**	**0.77**	0.006
LQR2COO	**0.59**	**0.70**	**0.90**	**0.82**	**0.75**	0.016	**0.58**	**0.71**	**0.74**	**0.94**	**0.74**	0.018

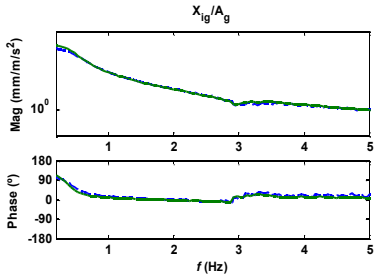

(a)

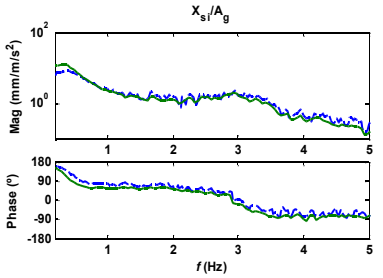

(b)

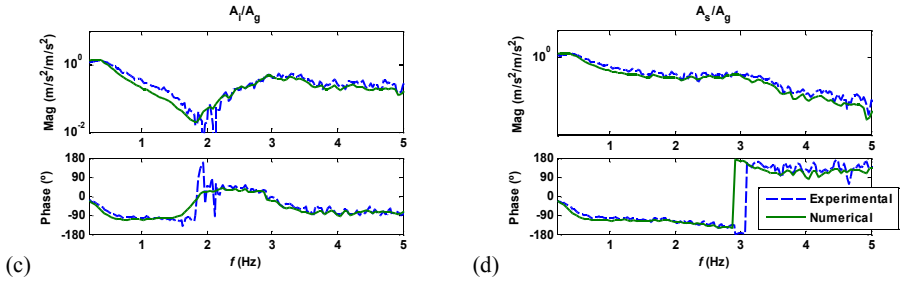

Fig. 4. Comparison between the numerical and experimental FRFs for the ICOO strategy: (a)-(b) relative displacements; (c)-(d) accelerations.

Some differences were found between the numerical and experimental data. However they follow the same trends. LQR2COO is the best performer and ICOO is the following one. ICOO is an interesting solution if a collocated control is employed. For this strategy in particular, a comparison between the experimental and numerical FRFs are presented in Fig. 4, showing a good agreement in general terms. Although, slightly differences on the magnitude of the first mode of vibration in terms of relative displacements can be observed. Anyway, the modal quantities, frequencies and damping ratios are very close to each other.

5. Conclusions

Several control strategies have been used for a comparative analytical and experimental study on a 2DOF system equipped with a MR damper. The overall objective was to validate the effectiveness of the proposed control strategies in reducing the responses of base-isolated structures when subjected to earthquake loads. Firstly, the mechanical system as well as the MR damper were modeled, and good agreement between the numerical and experimental data was found. Then the proposed controllers were tuned using the identified models and a set of representative ground motions. Finally, numerical and experimental trials were performed and similar performance trends were found. The passive case at maximum damping showed to be the best in reducing the base relative displacement but at the expense of increasing the other responses. The SA strategies performed better than the best passive case, and the LQR2COO exhibited the best performance, followed by the ICOO strategy. These one should be selected if collocated control is required. The results demonstrate that SA systems are viable for this subject.

References

[1] F. Casciati, J. Rodellar, U. Yildirim U, Active and semi-active control of structures – theory and applications: A review of recent advances, Journal of Intelligent Material Systems and Structures 23 (2012) 1181-1195.
[2] T.T. Soong, G.F. Dargush, Passive Energy Dissipation Systems in Structural Engineering, John Wiley & Sons Ltd., Chichester, 1997.
[3] A.K. Chopra, Dynamics of Structures: Theory and Applications to Earthquake Engineering, 2nd edn, Prentice-Hall, New York, 1995.
[4] A. Bahar, F. Pozo, L. Acho, J. Rodellar, A. Barbat, Hierarchical semi-active control of base-isolated structures using a new inverse model of magnetorheological dampers, Computers and Structures 88 (2010) 483-496.
[5] H.P. Gavin, U. Aldemir, Optimal Control of Earthquake Response Using Semiactive Isolation, Journal of Engineering Mechanics (ASCE) 131 (2005) 769-776.
[6] B.F. Spencer Jr., S. Nagarajaiah, State of the Art of Structural Control, Journal of Structural Engineering (ASCE) 129 (2003) 845-856.
[7] M.D. Symans, M.C. Constantinou, Semi-active control systems for seismic protection of structures: a state-of-the-art review, Engineering Structures 21 (1999) 469-487.
[8] S.J. Dyke, B.F. Spencer Jr., A comparison of semiactive control strategies for the magnetorheological dampers," Proceedings of the International Conference on Intelligent Information Systems (IIS '97), Grand Bahama Island, Bahamas, 1997, pp. 580-584.
[9] N. Luo, J. Rodellar, J. Vehí, M. De la Sen, Composite semiactive control of a class of seismically excited structures," Journal of the Franklin Institute 338 (2001) 225-240.
[10] H. Jung, K. Min Choi, B.F. Spencer Jr., I. Lee, Application of some semi-active control algorithms to a smart base-isolated building employing MR dampers, Structural Control and Health Monitoring 13 (2006) 693-704.
[11] H. Komatsu, Y. Shinozaki, Y. Sanui, R. Maseki, K. Yoshida, Y. Kitagawa, J. Toyama, I. Nagashima, A building with semi-active base isolation using sliding mode control, Proceedings of SMSST'07, World Forum on Smart Materials and Smart Structures Technology, Chongqing & Nanjing, China, 2007, pp.523-524.

[12] M. Zapateiro, H.R. Karimi, N. Luo, B.F. Spencer Jr., Real-time hybrid testing of semiactive control strategies for vibration reduction in a structure with MR damper, Structural Control and Health Monitoring 17 (2010) 427-451.
[13] D. Shook, P. Lin, T. Lin, P.N. Roschke, A comparative study in the semi-active control of isolated structures, Smart Materials and Structures 16 (2007) 1433-1446.
[14] N. Aguirre, F. Ikhouane, J. Rodellar, Proportional-plus-integral semiactive control using magnetorheological dampers, Journal of Sound and Vibration 330 (2011) 2185-2200.
[15] A. Rodríguez, F. Pozo, A. Bahar, L. Acho, Y. Vidal, J. Rodellar, Force-derivative feedback semi-active control of base-isolated buildings using large-scale MR fluid dampers, Structural Control and Health Monitoring 19 (2012) 120-145.
[16] B. F. Spencer Jr., S. J. Dyke, M. K. Sain, J. D. Carlson, Phenomenological model for magnetorheological dampers, Journal of Engineering Mechanics 123 (1997) 230-238.
[17] F. Oliveira, P. Morais, A. Suleman, Predictive Control for Earthquake Response Mitigation of Buildings Using Semi-active Fluid Dampers, Shock and Vibration Journal 14 (2014) 14 pages, Article ID 670683, http://dx.doi.org/10.1155/2014/670683.
[18] S. Narasimhan, S. Nagarajaiah, E.A. Johnson, H.P. Gavin, Smart base-isolated benchmark building. Part I: problem definition, Structural Control and Health Monitoring 13 (2006) 573-588.